THE ROLE OF THE ARGON AND HELIUM BATH GASES ON THE DETONATION STRUCTURE OF H_2/O_2 MIXTURE

Farzane Zangene[1], Zekai Hong[2], Qiang Xiao[3] and, Matei Radulescu[4]
[1] Mechanical Engineering, University of Ottawa, Ottawa, Canada, fzang055@uottawa.ca
[2] National Research Council of Canada, Ottawa, Canada, Zekai.Hong@nrc-cnrc.gc.ca
[3] Nanjing University of Science and Technology, Nanjing, China, qxiao@njust.edu.cn
[4] Mechanical Engineering, University of Ottawa, Ottawa, Canada, matei@uottawa.ca

ABSTRACT

Recent modeling efforts of non-equilibrium effects in detonations have suggested that hydrogen-based detonations may be affected by vibrational non-equilibrium of the hydrogen and oxygen molecules effects which could explain discrepancies of cell sizes measured experimentally and calculated without relaxation effects. The present study addresses the role of vibrational relaxation in $2H_2/O_2$ detonations by considering two-bath gases, argon and helium. These two gases have the same thermodynamic and kinetic effects when relaxation is neglected. However, due to the bath gases differences in molecular weight and reduced mass differences which affect the molecular collisions, relaxation rates can be changed by approximately 50-70%. Experiments were performed in a narrow channel in mixtures of $2H_2/O_2/7Ar$ and $2H_2/O_2/7He$ to evaluate the role of the bath gas on detonation cellular structures. The experiments showed differences in velocity deficits and cell sizes for experimental conditions keeping the induction zone length constant in each of the mixtures. These differences were negligible in sensitive mixtures but increased with the increase in velocity deficits while the cell sizes approaching the channel dimensions. Near the limits, differences of cell size in two mixtures approached a factor of 2. These differences were however reconciled by accounting for the viscous losses to the tube walls, evaluated using a modified version of Mirels' laminar boundary layer theory and generalized Chapman-Jouguet theory for eigenvalue detonations. The experiments suggest that there is an influence of relaxation effects on the cellular structure of detonations, which is more sensitive to wall boundary conditions. However, the previous works showed that the impact of vibrational non-equilibrium in a mixture of H_2/Air is more visible due to the effects of N_2 in the air, slowest to relax. Previous discrepancies suggested to be indicative of relaxation effects should be re-evaluated by the inclusion of wall loss effects.

1.0 INTRODUCTION

Detonation waves are known to have a cellular structure [1]. Recent numerical work found discrepancies between the predicted cell sizes and those measured experimentally. Taylor and others have attributed these discrepancies to the non-equilibrium effects in the detonation structure [2-3]. These effects have been argued to lengthen the ZND, Zeldovich-Von Neumann-Doering, structure and cell size. Xiao and Radulescu [4] also indicated that wall losses, usually not accounted for in the simulations, could also account for these discrepancies in the calculated cell size and measured experimentally. The presence of boundary layer losses in the experiments makes the detonation wave travel with a velocity less than the ideal Chapman-Jouguet (CJ) detonation velocity [5] and can lead to substantially larger cell sizes.

In the present work, we study the effect of different bath gases in H_2/O_2 detonations' structure. We consider two mono-atomic diluents, argon and helium, because, according to the ZND theory, the "equilibrium" chemical kinetics and hydrodynamics are not affected by the diluent. The detonations with either of the diluents have the same compressibility, energy release, shock temperature, and kinetics sensitivity to the shock state. However, the bath gas's molecular weight is known to impact the relaxation time of different molecules through the reduced mass effect [6]. By keeping the induction zone length constant in the experiments for the two bath gases, the cell size should remain constant under lossless conditions, and differences can be monitored and serve to explain the roles of

vibrational relaxation on the kinetics and the role of wall losses. This provides an unambiguous method to evaluate the influence of relaxation effects and wall losses on the structure of detonations.

2.0 EXPERIMENTAL SETUP

The experiments were performed in a rectangular shock tube that is 3.4m long, 0.203m height, and 0.019m width. The channel consists of initiation, propagation, and test section, which were made of aluminum [7]. The test section of the shock tube has glass walls for visualization; propagation of detonation wave is recorded in this section by a Phantom v1210 camera at 77481 frames per second with 0.468μs exposure time and 384×288 pixels resolution. A Z-type schlieren setup [8] consists of a slit, a vertical knife-edge, a 360Watt light source, and two concave mirrors to visualize propagation of detonation in the test section of the shock tube by recording refraction of the rays of light.

In all the experiments, a stoichiometric mixture of ethylene is used as the driver gas to initiate detonation. Many pilot tests had been done to avoid an overdriven detonation wave in the test section due to the high-pressure driver gas, and the lowest pressure that initiated detonation waves was determined. The ratio of 2.37 between driver gas and test gas was kept constant in all the experiments as the reference for filling the shock tube. The shock tube was evacuated to a pressure below 70Pa before filling it with driver and test gases. Eight high-frequency piezoelectric PCB pressure sensors were installed on the shock tube's top wall to record pressure signals. The global average propagation speed was obtained by the distance between the first and last pressure sensor divided by the time difference of these two pressure signals. The average of the repeated experiments' global velocity was considered the detonation velocity and used in calculations. By measuring the time it took for detonation to travel between the first and the last pressure sensors and knowing the distance between the two sensors, x= 125 cm, the detonation velocity in each experiment is calculated. The reported velocity is the average of the calculated velocity with the above-mentioned method of all the repeated experiments. The maximum deviation between the reported velocity and each experiment's velocity is considered the uncertainty of the experiments.

In table 1, the experimental conditions are explained, in which $2H_2/O_2/7Ar$ and $2H_2/O_2/7He$ mixtures are test gases. In the experiments, the induction zone length was kept constant between the helium diluted and argon diluted mixtures by changing the initial pressure of each test gas based on the ZND calculation. Two sets of induction zones were tested, with the largest induction zones corresponding to cell sizes comparable to the channel height. This corresponds to the limit in our experimental technique of comparing the cell size in the two mixtures for the same induction lengths. Table 1 shows the experimental test matrix in which pressures 4.1 kPa and 9.3 kPa are used for experiments in which the size of the cell will be larger and induction zone length expected to be the same based on ZND calculations for argon and helium dilutions. Similarly, pressures 7.2 kPa and 15 kPa will give the same induction zone length for the argon and helium dilutions with the smaller size of the cells due to the increase in initial pressure. In all the experiments, the temperatures are the same.

Table 1. Experimental mixtures and conditions

Test Mixture	P_0 [kPa]	T_0 [K]	Driver gas mixture	P_0 [kPa]	T_0 [K]
$2H_2+O_2+7Ar$	4.1	295	$C_2H_4+3O_2$	9.71	295
$2H_2+O_2+7He$	9.3	295	$C_2H_4+3O_2$	22.04	295
$2H_2+O_2+7Ar$	7.2	295	$C_2H_4+3O_2$	17.06	295
$2H_2+O_2+7He$	15	295	$C_2H_4+3O_2$	35.55	295

In order to determine the desired operating conditions, the variation of the induction zone length with pressure was calculated via ZND calculations of the steady lossless detonation structure [9].

Fig. 1 shows, for example, the corresponding ZND structures of the four mixtures tested. As usual, the point in the post-shock region in which thermicity is maximum is considered as the end of the induction zone. In the lower-pressure cases, the measured induction zone length is 2.83mm, and it is 1.6mm in the higher-pressure cases. From detonation theory, there is a classical correlation between cell size and induction zone length, $\lambda = A.\Delta_i$, in which the proportionality constant, A, comes from either experiments or simulations by using Euler equations. Therefore, by keeping the induction zone

length constant, we expect to observe the same cellular structure between two mixtures in the lower-pressure experiment and the same structure between two gases in the higher-pressure experiments.

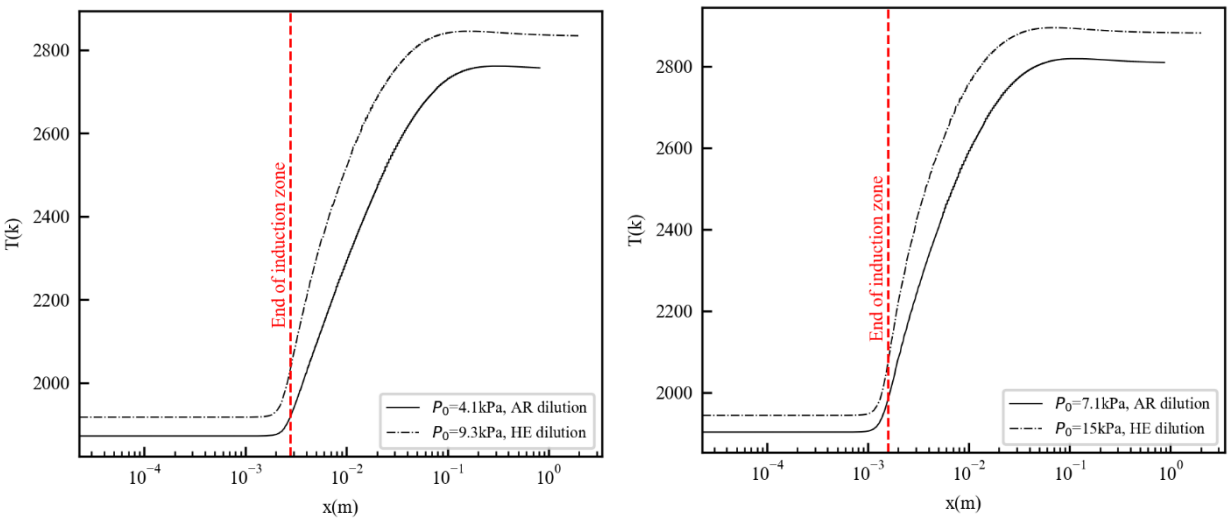

Figure 1. The evolution of the temperature with distance in the post-shock region was calculated from the ideal ZND model in the shock reference frame in the lower-pressure experiment (left) and higher-pressure experiment (right) experimental conditions.

3.0 EXPERIMENTAL RESULTS

3.1 Lower-pressure experiment

Fig. 2 represents the superimposed schlieren photos of a sequence of frames. This figure shows the evolution of the detonation front along the shock tube for the mixture of $2H_2/O_2/7Ar$, p_0 = 4.1kPa in the left and $2H_2/O_2/7He$, p_0 = 9.3kPa in the right. Each of these experiments was repeated five times in order to have an accurate and more reliable result. The detonation propagated from right towards left with the average global velocity of 1289m/s, 3090m/s for the argon and helium diluted mixtures, respectively. The cells' size in the argon diluted mixture is 203mm (Fig. 2, left) which is larger than 94mm in the helium diluted mixture (Fig. 2, right).

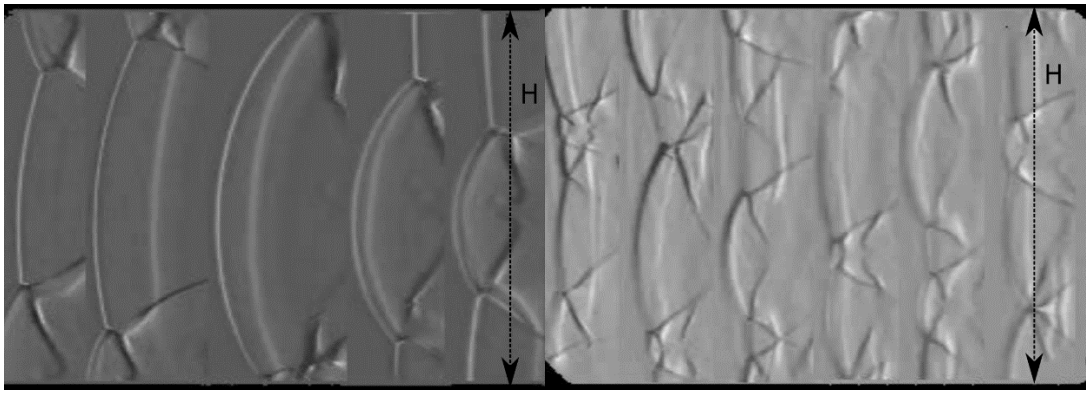

Figure 2. Superposition of detonation fronts at different instants along the shock tube in the mixture of $2H_2+O_2+7Ar$ (left) at an initial pressure of P_0 = 4.1kPa, and in the mixture of $2H_2+O_2+7He$ (right) at an initial pressure of P_0 = 9.3kPa, H is the channel height of 203mm.

3.2 Higher-pressure experiment

Fig. 3 presents the superposition of sequential frames of detonation propagation process from left to right for higher initial pressures, 7.2kPa for the argon diluted mixture, and 15kPa for the helium diluted mixture. The average velocity calculated from repeated experiments for the argon diluted

mixture is 1436m/s and for the helium diluted is 3350m/s. The cells' size decreased due to the increase of initial pressure, which is 58mm (Fig. 3, left) for the argon and 54mm for the helium mixtures (Fig. 3, right).

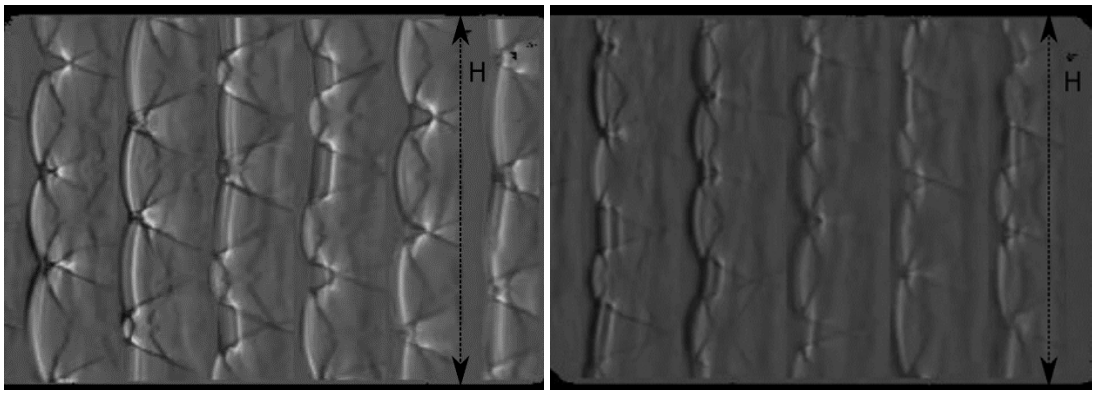

Figure 3. Superposition of detonation fronts at different instants along the shock tube in the mixture of $2H_2+O_2+7Ar$ (left) at an initial pressure of P_0 = 7.2kPa, and in the mixture of $2H_2+O_2+7He$ (right) at an initial pressure of P_0 = 15kPa, H is the channel height of 203mm.

Table 2. Experimental result

	P_0 [kPa]	D/D_{CJ}	Cell Width[mm]
$2H_2+O_2+7Ar$	4.1	0.8	203
$2H_2+O_2+7He$	9.3	0.86	94
$2H_2+O_2+7Ar$	7.2	0.89	58
$2H_2+O_2+7He$	15	0.9	54

Table 2 shows the summary of recorded velocity deficits, D/D_{CJ}, and cell width for the mixtures tested. Every two triple points (TP) is a cell, and the height of the channel is 203 mm. We can measure the cell width of each experiment by counting the number of triple points in each frame on the recorded video and average the calculated number of TPs in all the frames in each experiment. Finally, the reported cell width is the average over all the repeated experiments for the same mixture. The global velocity, D, the calculation is explained in section 2, and CJ speed velocity, $D_{CJ,}$ is calculated from the ZND model with losses which is explained in the following section, 5.

The experimental measurements of the cell width show that the difference between the argon and helium in the lower-pressure experiment is approximately 53% and 7% in the higher-pressure experiments. Hence, the detonation waves' cellular structure in the argon and helium diluted mixtures do not have the same size as the cell, mainly in the lower-pressure experiments. This observation raises the question: Is the discrepancy because of the difference in vibrational non-equilibrium effects present in the experiment or because of the effect of losses inside the shock tube? In the next sections, we try to address this question by estimating the characteristic vibrational relaxation times and boundary layer losses calculations.

4.0 VIBRATIONAL NON-EQUILIBRIUM EFFECT

In order to evaluate the relative influence of helium and argon as bath gases for vibrational relaxation, we have to evaluate the characteristic relaxation times of H_2 and O_2 molecules. While many other molecules are present during the decomposition, these time scales should indicate the magnitude of the relaxation times and the relative influence of the helium and argon bath gases. Equation 1 is used for computing the vibrational relaxation time of each of the species τ_i in the mixture of N gases based on the contributions of collisions with the species itself and other species, which comes from fitting experimental data by a least square procedure [10]

$$\frac{1}{P\tau_i} = \sum_{j=1}^{N} \frac{X_j}{P\tau_{i-j}} \quad (1)$$

In the above relation, $P\tau_i$ has the unit of *atm.s*, and τ_{i-j} is the vibrational relaxation time of species *i* diluted in species j, and *Xj* is the mole fraction of species j. Therefore, τ_i is the total vibrational relaxation time of species *i* in the whole mixture, while τ_{i-j} is only the vibrational relation time of specie *i* with species *j* and not the effect of the overall mixture. Therefore, for the two desired mixtures, the vibrational relaxation time of hydrogen and oxygen with other molecules in the mixture can be calculated by:

$$\frac{1}{P\tau_{O_2}} = \frac{X_{\mathrm{H_2}}}{P\tau_{\mathrm{O_2-H_2}}} + \frac{X_{\mathrm{O_2}}}{P\tau_{\mathrm{O_2-O_2}}} + \frac{X_{\mathrm{diluent}}}{P\tau_{\mathrm{O_2-diluent}}}$$

$$\frac{1}{P\tau_{\mathrm{H_2}}} = \frac{X_{\mathrm{H_2}}}{P\tau_{\mathrm{H_2-H_2}}} + \frac{X_{\mathrm{O_2}}}{P\tau_{\mathrm{H_2-O_2}}} + \frac{X_{\mathrm{diluent}}}{P\tau_{\mathrm{H_2-diluent}}} \quad (2)$$

In which $X_{\mathrm{H_2}}: 0.2$, $X_{\mathrm{O_2}}: 0.1$, $X_{\mathrm{diluent}} : 0.7$. To calculate $P\tau_{\mathrm{H2-j}}$, we use the empirical relations from [10]:

$$\log p\tau_{\mathrm{H2-H2}} = (34.74 \pm 0.16)T^{-\frac{1}{3}} - (8.686 \pm 0.012)$$

$$\log p\tau_{\mathrm{H2-He}} = (41.35 \pm 0.8)T^{-\frac{1}{3}} - (8.984 \pm 0.063) \quad (3)$$

$$\log p\tau_{\mathrm{H2-Ar}} = (45.09 \pm 0.56)T^{-\frac{1}{3}} - (8.956 \pm 0.044)$$

Due to the lack of experimental data for the relaxation time of H_2 in O_2, we used the relaxation time of H_2 in Ar instead, considering molecular weights for these two molecules are close (Ar:40 AMU, O_2: 32 AMU). To calculate $P\tau_{O2-j}$, we can use the Landau-Teller harmonic oscillator model [2], which is valid for many diatomic species:

$$P\tau(T) = \exp\left[A\left(T^{-\frac{1}{3}} - B\right) - 18.42\right] \quad (4)$$

in which from experimental measurement, for O_2-O_2, A = 133 and B = 0.03, and for O_2-H_2, A = 36 and B= 0.000067. For the relaxation time of O_2-Ar and O_2-He, we directly use the experimental result because Landau-Teller harmonic oscillator model is only valid for diatomic species. Therefore, $P\tau_{\mathrm{O2-Ar}}$ and $P\tau_{\mathrm{O2-He}}$ are 0.0007, 0.0002 respectively [6]. The results of our vibrational relaxation time scales for the $2H_2/O_2/7Ar$ and $2H_2/O_2/7He$ in different initial pressure are presented in table 3. Additionally, ignition delay time computed by using a realistic chemistry ZND calculation for detonation wave in two mixtures is presented in table 3 to have a qualitative comparison. For these calculations, *P* and *T* are post-shock state pressure and temperature for each of these mixtures.

Table 3. Vibrational relaxation time and ignition delay time

	p_0[kPa]	τ_{H2}[s]	τ_{O2}[s]	τ_{ignition}[s]	$\frac{\tau_{\mathrm{ignition}}}{\tau_{\mathrm{H2}}}$	$\frac{\tau_{\mathrm{ignition}}}{\tau_{\mathrm{O2}}}$
$2H_2+O_2+7Ar$	4.1	3.06×10^{-6}	8.5×10^{-7}	7.2×10^{-6}	2.34	8.4
$2H_2+O_2+7He$	9.3	8.14×10^{-7}	3.5×10^{-7}	3.2×10^{-6}	3.92	8.9
$2H_2+O_2+7Ar$	7.2	1.64×10^{-6}	4.7×10^{-7}	4.1×10^{-6}	2.4	8.7
$2H_2+O_2+7He$	15	4.8×10^{-7}	2.15×10^{-7}	1.8×10^{-6}	3.74	8.3

Firstly, the relaxation times with helium dilution are approximately 50-70% shorter than the argon dilution. Secondly, our estimations show that the H_2 molecule relaxes on a time scale more comparable to the ignition delay time. These results illustrate that relaxation time scales may be comparable to the characteristic time scales of a detonation. While the unsteadiness associated with

the cellular structure gives rise to a variation of the ignition delay time by several orders of magnitude, the time associated with the residence time in the hydrodynamic thickness of detonations is also approximately two orders of magnitude longer than the induction time [11]. These estimates show that vibrational relaxation effects operate on relevant time scales, and differences between argon and helium dilution can account for 50-70% changes in these time scales.

5.0 BOUNDARY LAYER LOSSES CALCULATION

The differences in the wall losses for the two diluents were evaluated in the framework of quasi-1D ZND detonations with flow divergence to the boundary layers [4]. The boundary layer displacement thickness was estimated using Mirels' theory for laminar boundary layers behind steady shock waves. The non-constant flow in the reaction zone was accounted for through a modified growth rate of the boundary layer for accelerating flows. The Euler governing equations for the steady, inviscid, reactive quasi-1D flow in the shock attached reference frame are [12]

$$\frac{dp}{dt'} = -\rho u^2 \frac{\dot{\sigma}-\dot{\sigma}_A}{1-M^2} \tag{5}$$

$$\frac{du}{dt'} = u\frac{\dot{\sigma}-\dot{\sigma}_A}{1-M^2} \tag{6}$$

$$\frac{d\rho}{dt'} = -\rho\frac{\dot{\sigma}-M^2\dot{\sigma}_A}{1-M^2} \tag{7}$$

$$\frac{dx'}{dt'} = u \tag{8}$$

Where p, ρ, u are the mixture pressure, density, velocity, and *M* is the Mach number of the flow. For a mixture of ideal gases, the thermicity reduces to the equation 9:

$$\dot{\sigma} = \sum_{i=1}^{N_s}\left(\frac{W}{W_i} - \frac{h_i}{c_pT}\right)\frac{dy_i}{dt'} \tag{9}$$

In which W_i, Y_i, h_i are molecular weight, mass fraction as well as enthalpy of ith species; and W, c_pAnd T are the mean molecular weight, specific heat, and temperature of the mixture. The kinetics for the evolution of the mass fractions, *Yi*, of each of the species is obtained from the below equation:

$$\frac{dY_i}{dt'} = \frac{W_i\dot{\omega}_i}{\rho} \tag{10}$$

In equation 10, $\dot{\omega}_i$ is the molar production rate of species *i*. The lateral strain rate of the flow in the channel is calculated by,

$$\dot{\sigma}_A = u\frac{1}{A}\frac{dA}{dx'} \tag{11}$$

$$\frac{d}{dx'}(\ln A) = \frac{K_M}{w+2\delta^*(x')} \times \frac{d\delta^*(x')}{dx'} \tag{12}$$

In which δ^* is boundary layer negative displacement thickness, *w* is the physical channel width of 19mm. The simulations of Xiao et al. [4] have shown that the real boundary layer is thinner than that predicted by Mirels' model [13], as Mirels assumed uniform flow behind the leading shock. However, for detonations, the flow is not uniform and accelerates in the shock attached frame with steep pressure and temperature gradients. Hence, the effect of the boundary layer's negative displacement thickness is presented by applying a modification to Mirels' compressible laminar boundary layer growth rate. The corrected negative displacement thickness becomes:

$$\delta^* = K_M\sqrt{\nu\int_0^{x'}\frac{dx'}{u(x')}} \tag{13}$$

where the term in the integral represents the time elapsed for a fluid particle to reach a position x' behind the lead shock. In the equation 13, ν is the kinematic viscosity of the mixture in the post-shock region and K_M is Mirels' constant [13], which has a significant dependency on the mixture compositions and minor dependency on initial pressure. The detailed computation of this constant is available on the work of Xiao and Radulescu [4]. Table 4 presents the result of detailed calculations of K_M based on our experimental conditions.

Table 4. Mirel's constant for experimental condition

	P_0 [kPa]	K_M
$2H_2+O_2+7Ar$	4.1	4.09
$2H_2+O_2+7Ar$	7.2	4.11
$2H_2+O_2+7He$	9.3	3.8
$2H_2+O_2+7He$	15	3.82

For each mixture and initial state, the detonation speed and reaction zone structure were obtained by a shooting method for the speed eigenvalue. The correct speed was such that the generalized CJ condition was satisfied inside the reaction zone, where the flow becomes sonic as the rate of energy release balances the rate of the loss. Fig. 4 shows the evolution of temperature in post-shock for all four experimental conditions. It can be observed that the induction zone length, Δ_i, becomes longer due to the decrease in the initial pressure. Unlike the result of the ZND calculation with no loss, in Fig. 1 section 2, here Fig. 4 shows that the induction zone does not have the same length for the argon and helium dilution. In lower-pressure calculations, close to the limit, the effect of lengthening in the reaction zone reduces the velocity of the wave; the larger the velocity deficit, the larger the size of the cell's width. The calculated induction zone lengths for both mixtures are reported in table 5.

Table 5. Induction zone length measured by ZND model with losses.

	P_0 [kPa]	Δ_i [m]
$2H_2+O_2+7Ar$	4.1	0.012
$2H_2+O_2+7Ar$	7.2	0.0029
$2H_2+O_2+7He$	9.3	0.0057
$2H_2+O_2+7He$	15	0.0023

The difference between induction zone lengths in the higher-pressure experiments is 20%, while in the lower-pressure experiments, this difference is 52% which is compatible with the experimental observations in the previous section.

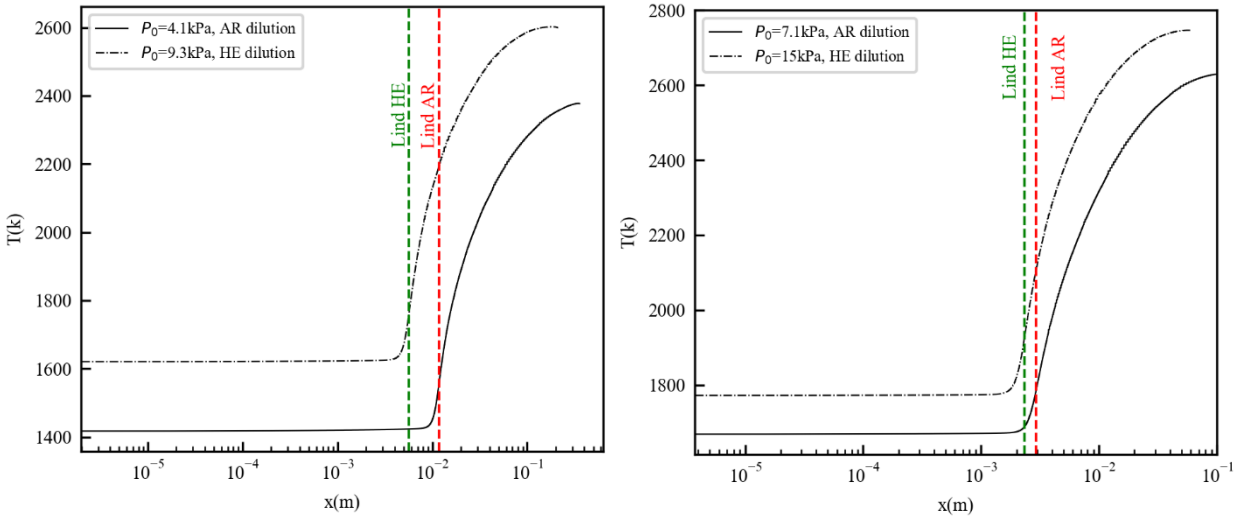

Figure 4. The evolution of the temperature with distance in post-shock region calculated from ZND model with losses in the shock reference frame in the lower-pressure experiment(left) and the higher-pressure experiment(right).

We measured the induction zone length using a ZND model with and without boundary layer losses. In Fig. 5, the solid line represents the changes of nondimensional Δ_i from loss calculation with nondimensional Δ_i from ideal ZND calculation versus ideal Δ_i, nondimensionalized with channel width. The solid line shows the argon diluted mixture, and the dashed line is for the helium diluted mixtures.

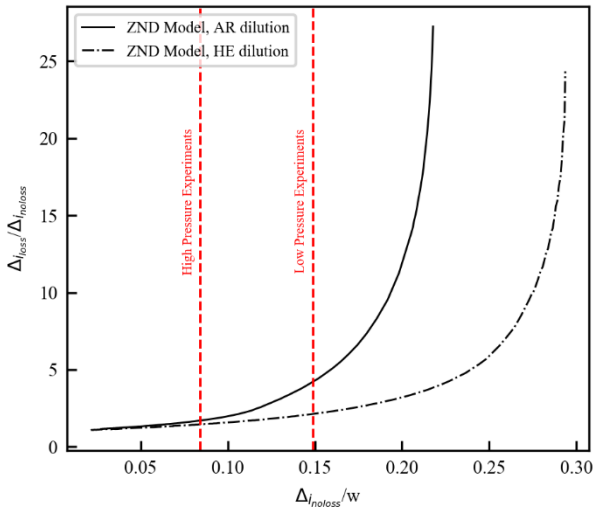

Figure 5. The evolution of nondimensional induction zone length from ZND model with losses versus nondimensional induction zone length from ZND model without losses

6. DISCUSSION

The ratio of induction zone length of the argon diluted over the helium diluted mixtures calculated by the ZND model with losses and comparison with experimental measurement of cell width is presented in Fig. 6. The blue circle is the cell width ratio in both argon and helium dilution in the higher-pressure experiment with a 0.18 standard deviation ratio (SDR), the blue error bar, and the green circle is related to the same ratio in the lower-pressure experiments with 0.3 SDR, the green error bar. This graph shows that the ZND model with losses can predict the experimental result with very good accuracy, less than 9% error in both higher- and lower-pressure experiments. This result explains why the cell width in the lower-pressure experiments is not precisely the same, and it is because of the higher losses near the limit [4].

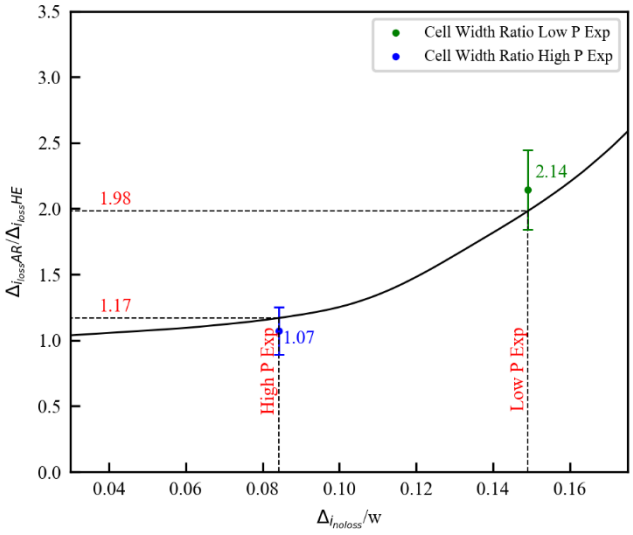

Figure 6. The ratio of the argon dilution induction zone length from ZND model with losses and helium versus nondimensional induction zone length from ZND model without losses

In Fig. 7, the numerically calculated velocity deficits of both mixtures versus nondimensionalized induction zone length without loss and velocity deficit measured from experiments are presented. In lower-pressure experiments, the velocity deficits are higher.

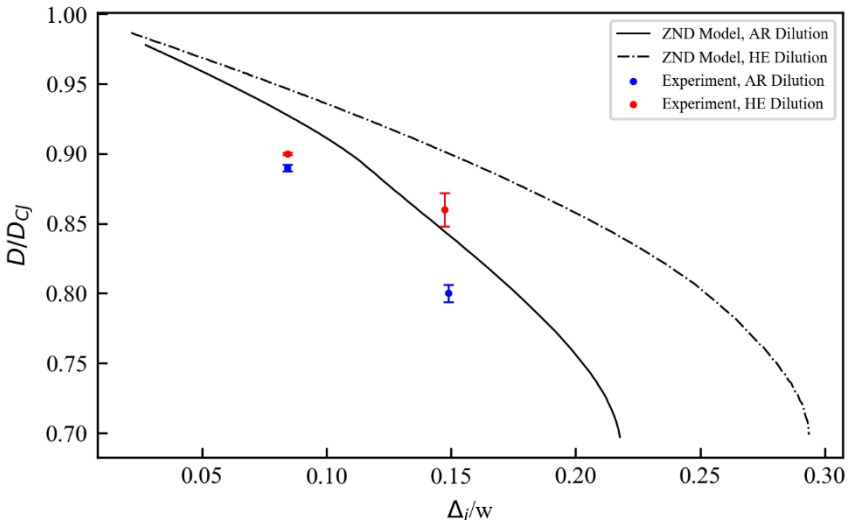

Figure 7. The mean propagation velocity in argon and helium mixtures was measured experimentally (circles) and calculated from the ZND model with losses (lines); the abscissa is the inverse channel thickness normalized by the induction zone length at CJ conditions.

The error bars are experimental uncertainty calculated between repeated experiments. For the higher-pressure experiment, 0.2% in the argon and 0.07% in the helium as well as 0.63% and 1.2% for the lower-pressure experiments in the argon and helium, are calculated. Table 6 represents a quantitative comparison between velocity deficits measured in experiments with those calculated from the ZND model.

Table 6. Velocity deficit measured from experiment and ZND

	P_0 [kPa]	$\frac{D}{D_{CJ}}$ (Exp)	$\frac{D}{D_{CJ}}$ (Numerical)	Error%
$2H_2+O_2+7Ar$	4.1	0.8	0.84	5
$2H_2+O_2+7He$	9.3	0.86	0.9	4.6
$2H_2+O_2+7Ar$	7.2	0.89	0.92	3.3
$2H_2+O_2+7He$	15	0.9	0.95	5.5

In the helium diluted experiments, the deviation between the ZND model and experimental results is higher. Hence, the ZND model is not predicting the experimental result accurately, which can be the effect of vibrational non-equilibrium that we did not consider in chemical calculation or the effect of cellular structure or, more likely, the current ZND model is not the perfect model to predict the experimental result. More realistic numerical simulation of cellular detonation with losses needs to be done to have a more accurate model.

The above analysis has quantitatively shown that argon dilutions' relaxation times are approximately 50-70% longer than the helium dilution due to the larger reduced mass of argon. Additionally, boundary layer analysis showed that due to the higher velocity deficit in the argon mixture, the cells' size is 52% and 20% larger than the helium mixture in the lower and higher-pressure experiments. Moreover, we measured 53% and 7% larger cells' size for the lower and higher-pressure experiments with argon diluted mixtures compared to the helium diluted from experimental observation. All the results are in good agreement and reveal that close to the limit, lengthening in the reaction zone reduces the velocity of the wave, which causes the discrepancy in the size of the cells between two mixtures. However, in the higher-pressure experiments shorter reaction zone causes less velocity deficit and less difference between the cellular structures whether the diluent is argon or helium. Therefore, within the accuracy of the experiments, vibrational non-equilibrium effects in the higher-

pressure experiments are not evident. Closer to the limits, every small potential effect is amplified by the losses, which permits us to better see the differences in relaxation effects. It means that if there is a small effect of lengthening the reaction zone because of non-equilibrium vibrational mode, these effects through the nonlinear coupling with the losses will reduce the velocity of the wave, reduce reactions, and further amplifies the impact. The ~ 5% differences evident when comparing detonation velocity deficits with model prediction require further evaluation, using more sophisticated models to incorporate the effect of losses and relaxation on cellular detonations.

7.0 CONCLUSION

The reaction zone cellular structure of $2H_2/O_2$ detonation was found to be affected by the type of monoatomic diluent when propagating in thin channels. 70% argon dilution detonations were found to yield cell sizes larger by a factor of 2 than those with 70% helium dilution, while the velocity deficits were also larger for the argon mixture. Taylor [2] calculated the vibrational relaxation time in a stoichiometric mixture of H_2/Air in atmospheric pressure and showed that due to the presence of N_2 in air, greater self-relaxation time than other species in the mixture, vibrational relaxation times are more affected by vibrational non-equilibrium produced by shock waves. Our calculations for $2H_2/O_2$ in pressures ten times less than Taylor's calculations showed that the reduced mass effects in the molecular collision could account for part of characteristic relaxation times differences in the reaction zone. Furthermore, the account of the transport properties and wall losses reduced the differences below the experimental uncertainty. We thus conclude that vibrational relaxation effects in detonations in narrow channels fall within the experimental noise when differences in relaxation times are varied by up to 70%. It is, therefore, reasonable to say that vibrational non-equilibrium effects in the H_2 related mixtures make the prediction of the cell size difficult.

REFERENCES

1. Shepherd, J.E., Detonation in gases, *Proceedings of the Combustion Institute*, 32, 1, (2009) 83–98.
2. Taylor, B.D., Kessler, D.A., and Oran, E.S., Estimates of vibrational non-equilibrium time scales in hydrogen-air detonation waves, *Proceeding of 24th of ICDERS*, 189, 5, (2013), 841–853.
3. Taylor, B.D., Kessler, D.A., Gamezo V.N., and Oran E.S., Numerical simulations of hydrogen detonations with detailed chemical kinetics, *Proceedings of the Combustion Institute*, 34, 2, (2009), 2009–2016.
4. Xiao, Q. and Radulescu, M.I., Dynamics of hydrogen–oxygen–argon cellular detonations with a constant mean lateral strain rate, *Combustion and Flame*, 215, (2020), 437–457.
5. Xiao, Q., Sow A., Maxwell B., and Radulescu M.I., Effect of boundary layer losses on 2D detonation cellular structures, *Proceedings of the Combustion Institut*e, 38, 3, (2020), 3641–3649.
6. White, D.R., and Millikan R.C., Oxygen vibrational relaxation in oxygen–helium and oxygen–argon mixtures, *Journal of Chemical Phys*ics, 39, (1963), 1803.
7. Bhattacharjee, R.R., Experimental investigation of detonation re-initiation mechanisms following a mach reflection of a quenched detonation, Master thesis, University of Ottawa, (2013).
8. Settles, G.S., Schlieren and Shadowgraph Techniques, *Springer Berlin Heidelberg*, (2001).
9. Lawson J., and Shepherd J., Shock & Detonation Toolbox, California Institute of Technology, Pasadena, CA , (2019).
10. Dove, E., The vibrational relaxation of hydrogen, *Journal of Chemical Physics*, 81, 25, (1974), 2564–2572.
11. Lee, J.H.S., and Radulescu, M.I., On the Hydrodynamic Thickness of Cellular Detonations. *Combustion, Explosion, and Shock Waves*, 41,6, (2005), 745–765.
12. Radulescu M.I., and Borzou B., Dynamics of detonations with a constant mean flow divergence, *Journal of Fluid Mechanics*, 845, (2018), 346-377.
13. Mirels, H., Boundary layer behind shock or thin expansion wave moving into stationary fluid, NACA TN 3712 , (1956).